

Primary Electron Transfer Kinetics in Membrane-Bound *Rhodobacter sphaeroides* Reaction Centers: A Global and Target Analysis[†]

I. H. M. van Stokkum,^{*,‡} L. M. P. Beekman,[‡] M. R. Jones,[§] M. E. van Brederode,[‡] and R. van Grondelle[‡]

Faculty of Physics and Astronomy, Vrije Universiteit, Amsterdam, The Netherlands, and Krebs Institute for Biomolecular Research and Robert Hill Institute for Photosynthesis, Department of Molecular Biology and Biotechnology, University of Sheffield, Western Bank, Sheffield S10 2UH, United Kingdom

Received April 7, 1997; Revised Manuscript Received July 15, 1997[⊗]

ABSTRACT: Absorbance difference kinetics were measured on quinone-reduced membrane-bound wild type *Rhodobacter sphaeroides* reaction centers in the wavelength region from 690 to 1060 nm using 800 nm excitation. Global analysis of the data revealed five lifetimes of 0.18, 1.9, 5.1, and 22 ps and a long-lived component for the processes that underlie the spectral evolution of the system. The 0.18 ps component was ascribed to energy transfer from the excited state of the accessory bacteriochlorophyll (B^*) to the primary donor (P^*). The 1.9 ps component was associated with a state involving a BChl anion absorbing in the 1020 nm region. This led to the conclusion that primary electron transfer is best described by a model in which the electron is passed from P^* to the acceptor bacteriopheophytin (H_L) via the monomeric bacteriochlorophyll (B_L), with the formation of the radical pair state $P^+B_L^-$. An analysis assuming partial direct charge separation from B^* [Van Brederode, M. E., Jones, M. R., and Van Grondelle, R. (1997) *Chem. Phys. Lett.* 268, 143–149] was also consistent with the data. Within the framework of a five component model, the 5.1 and 22 ps lifetimes were associated with charge separation and relaxation of the $P^+H_L^-$ radical pair state respectively, providing a description which adequately accounted for the complex kinetics of decay of P^* . Alternatively, by assuming that the 5.1 and 22 ps components originate from a single component with a multi-exponential decay, a simpler analysis with only four components could be employed, resulting in only a small increase (7%) in the weighted root mean square error of the fit. In both descriptions part of the decay of P^* proceeds with a lifetime of about 2 ps. The relative merits of these alternative descriptions of the primary events in light-driven electron transfer are discussed. Similar measurements on YM210H mutant reaction centers revealed four lifetimes of 0.2, 3.1, and 12 ps and a long-lived component. The 3.1 and 12 ps lifetimes are ascribed to multi-exponential decay of the P^* state. The differences with the WT data are discussed.

The reaction center (RC) of purple bacteria is responsible for the conversion of light energy into a transmembrane electrical potential. The structures of the RC from two species of purple bacteria, *Rhodospseudomonas (Rps.) viridis* and *Rhodobacter (Rb.) sphaeroides*, have been solved to high resolution (1, 2). They reveal an assembly of protein subunits and redox cofactors that are arranged around an axis of approximate 2-fold symmetry. The primary donor of electrons (P) is a pair of excitonically-coupled bacteriochlorophyll *a* (BChl) molecules positioned close to the periplasmic face of the protein. The remaining redox cofactors, two monomeric BChls (B), two molecules of bacteriopheophytin *a* (H), and two ubiquinones (Q), are arranged around the symmetry axis in two branches that span the membrane dielectric. Excitation of P initiates a sequence of electron transfer reactions that result in the separation of charge across the inner membrane of the bacterium. Only P and the branch

of redox cofactors most closely associated with the L subunit of the RC (P, B_L , H_L and Q_A) are involved in the transmembrane electron transfer process (3–5). The role of the bacteriochlorin cofactors on the M subunit branch (B_M and H_M) is unclear.

In wild type RCs it is generally assumed that electron transfer is driven from the first singlet excited state of the primary donor (P^*), with the first clearly-resolved charge separated state being the radical pair $P^+H_L^-$. Experiments have shown that the lifetime of P^* is approximately 3.5 ps in detergent-solubilized RCs (4) and approximately 4.5 ps in membrane-bound RCs (6, 7). Time-resolved difference absorption spectroscopy can be used to follow the sequence of events in the first steps of transmembrane electron transfer. Such spectroscopy has shown that the decay of P^* into the charge-separated state $P^+H_L^-$ is accompanied by the appearance of an electrochromic bandshift of the 800 nm absorption which is thought to arise from the formation of an electric field between the P^+ and H_L^- radicals that affects the absorption properties of the intervening B_L BChl. The time-resolved spectra also show a bleach at 760 nm, attributed to the loss of ground state absorbance of H_L (3), and the appearance of the absorption band of an anionic species at 670 nm (8–10). All three spectral features develop with approximately the same time constant as the

[†] The investigations were supported by the Life Sciences Foundation (SLW), which is subsidized by the Netherlands Organization for Scientific Research (NWO) and by EC Contracts CT92-0796 and CT93-0278. M.R.J. is a BBSRC Advanced Research Fellow.

* Address correspondence to this author at Faculty of Physics and Astronomy, Vrije Universiteit, De Boelelaan 1081, 1081 HV Amsterdam, The Netherlands. Tel: 31 20 444 7868. FAX: 31 20 444 7899. E-mail: ivo@nat.vu.nl.

[‡] Vrije Universiteit, Amsterdam.

[§] Krebs Institute, Sheffield.

[⊗] Abstract published in *Advance ACS Abstracts*, September 1, 1997.

decay of P^* . However, extensive studies have shown that primary electron transfer is a complex process, and a number of questions concerning the details of the reaction mechanism remain to be answered. First, a wavelength dependence of the kinetics of the bandshift of the B absorption band has been observed (11). An additional time component has been assigned in this spectral region, and also around 1020 nm (12), that was attributed to the formation of B_L^- as an intermediate in the electron transfer process (8, 9). Furthermore, fluorescence emission from P^* has been found to decay with multiple time constants that extend from a few to hundreds of picoseconds (7, 12–20).

Much of the discussion concerning the first step in electron transfer in the bacterial RC has addressed the relative merits of two mechanisms that treat the role of the accessory BChl, B_L , in different ways. The first of these, often referred to as the superexchange mechanism, considers electron transfer from P^* to H_L to be a single-step reaction, with B_L involved as a virtual intermediate that enhances the electronic overlap between P and H_L (4, 5). The second mechanism involves the formation of the radical pair $P^+B_L^-$ as a discrete, but short-lived, intermediate in a two-step reaction from P^* to $P^+H_L^-$. The complexity of the optical changes accompanying primary electron transfer has lent much support to the idea that such intermediate charge separated states play a role in the reaction, and direct evidence for the formation of the $P^+B_L^-$ radical pair state has been presented (6, 8, 9, 12, 18, 21, 22).

A second point concerns the possible contribution of electron transfer from B_L^- or B_M^- , not involving P^* . In a *Rb. sphaeroides* mutant, YM210W, which exhibits ultraslow electron transfer from P^* in approximately 400 ps, at 77 K about 40% ultrafast charge separation without the involvement of P^* was clearly observed upon excitation of B (23, 24). In this alternative electron transfer pathway in approximately 6.5 ps clearly the formation of $P^+H_L^-$ was observed. On the basis of the time-gated spectra directly after the 0.2 ps ultrafast B^* relaxation process we suggested that in this electron transfer pathway $P^+B_L^-$ and $B^+H_L^-$ are directly formed from B^* which are then converted to $P^+H_L^-$. Similar electron transfer mechanisms might be operating in wild type RCs at room temperature, as was suggested by (20) on the basis of 15–20% less P^* stimulated emission formed upon excitation in the H and B band compared to excitation of the P band.

A third point of discussion has been the role of the protein environment in the electron transfer process. The exclusive use of the L cofactor branch for electron transfer has been ascribed to an effect of the protein (25–27) and site-directed mutagenesis has been used in attempts to activate the inactive cofactor branch, but with limited success (5, 26–31). The protein is also believed to influence the electron transfer process through its role as a glassy host for the redox cofactors participating in the reaction. Variation in the kinetics of electron transfer, such as deviations from mono-exponential behavior, could arise from slight variations in the structure of the protein-cofactor matrix which give rise to static inhomogeneity (11, 19, 32–37). In a different view of the role of the environment of the RC cofactors, the protein is envisaged as reacting to the ongoing electron transfer process, providing a dynamic environment within which electron transfer takes place. In this model, the charges

residing on the two halves of the radical pair are solvated by the protein, leading to a decrease in the free energy of the radical pair with time and an increase in the free energy gap between the P^* state and the charge separated state (18, 20, 38–40). Multi-exponential decay of the P^* state is viewed as arising from a decreased probability with time of recombination from the charge separated state to the P^* state, as the free energy gap between the two increases. In support of this dynamic solvation model, it is apparent that estimates of the size of the free energy gap derived from experiments conducted on the sub-nanosecond time scale are invariably smaller than estimates from data collected on longer time scales, an effect ascribed to relaxation of the $P^+H_L^-$ radical pair (33, 38). However, there is still some debate over whether additional components in the kinetics of P^* decay, on the time scale of tens of picoseconds, result from similar relaxation processes. It is also worth noting that these two roles for the protein are not mutually exclusive.

The data presented in this report address the role of B_L in the primary electron transfer reaction, and the complexity of the decay of the P^* state. Time-resolved absorption difference spectroscopy over the wavelength range 690–1060 nm has been applied to wild type membrane-bound *Rb. sphaeroides* RCs, in order to resolve the optical changes associated with the first step of the electron transfer process. The wavelength range investigated includes the region (960–1060 nm) in which absorption from B_L^- would be expected to be found (19, 20). A preliminary analysis of the 960–1060 nm data set has been presented elsewhere (41). Experiments were also conducted with membrane-bound RCs bearing the mutation Tyr M210→His. The data are examined by global and target analysis and are discussed in terms of the mechanism of primary electron transfer, and the relative merits of models invoking static distributions and relaxation processes as explanations for the complex decay of the P^* state.

MATERIALS AND METHODS

Samples of membrane-bound RCs from *Rb. sphaeroides* strain RCO1 and a YM210H mutant (42) were prepared as described previously (7, 42). Time-resolved absorption changes were measured in a rotating sample cell with 1.2 nJ pulses that excited the sample at 800 nm with a 250 kHz repetition rate resulting in an average power of 300 μ W. Both excitation and probe pulses were vertically polarized. The spectral changes were probed with a white light continuum generated from the same Ti-sapphire-based laser system (19). Under these conditions, and with a relatively large spot size of 100 μ m, 2–3% of the RCs were excited per excitation pulse. RCs were kept in an active state by pre-reduction of the quinone molecules with 100 mM sodium ascorbate (7). The probe wavelength was selected using a band-pass filter before the sample and a monochromator between the sample and the photodiode detector. This method of wavelength selection together with the fact that at various wavelengths the resolution of the monochromator was altered to increase the light intensity on the photodiode resulted in a small amount of wavelength imprecision and a reduced spectral resolution. Consequently a typical kinetic trace was an average over 5 nm.

A total of 97 kinetic traces were measured for wild type membranes in the wavelength range 690–1060 nm. Data

in the range 960–1060 nm were collected over a 20 ps time window with an instrument response of 0.18 ps (full width at half-maximum, FWHM). Data in the range 690–960 nm were collected over a 100 ps time window with an instrument response (FWHM) between 0.48 and 0.69 ps. Data collected for the YM210H mutant consisted of 55 kinetic traces in the 725–1050 nm range on a time scale of 50 ps with an instrument response (FWHM) of 0.44 ps. The instrument response was described by a Gaussian shape with two parameters for location and width. The location parameter was estimated for each trace, whereas the width parameter was estimated for each data set (consisting of consecutively measured traces). The data were analyzed using a global analysis program that is described in detail elsewhere (19, 43). Target analysis was performed in two ways: firstly, with compartmental models including back reactions which described the concentrations of the different species. Secondly, the multiexponential character of the P* stimulated emission decay was investigated. This result was then related to a heterogeneous, sequential compartmental model without back reactions. Details are described below.

A note should be made at this point concerning the scaling of the data. Since the filters, bandwidths, and wavelengths changed somewhat from trace to trace, the data were scaled afterwards in such a way that the later parts of the traces resemble the time gated spectra of the same preparations studied in (7). For wavelengths from 945–1060 nm the P⁺ spectrum from (44) was used to scale the estimated end spectrum (shown in Figure 2E or Figure 4D), assuming that this represents P⁺. Since the detection was not at magic angle some polarization effects (1, 19, 45) may be present in our spectra after this scaling. However, in particular for P and B these effects are expected to be small. The smooth curves drawn in the spectra were calculated using the approximating spline routine CSSCV (46).

RESULTS

Global Analysis of Light-Induced Absorption Changes in Membrane-Bound Wild Type RCs

In Figure 1 measured kinetics are shown at 775, 825, 925, and 1010 nm. The complexity of the absorption changes at these key wavelengths shows that a number of different processes contribute to the spectral evolution of the system. The kinetic data at all 97 wavelengths were analyzed globally yielding five lifetimes of 0.18, 1.9, 5.1, and 22 ps and a long-lived component. The contributions of each of these components to the fit to the raw kinetic data are depicted in Figure 1. The decay-associated difference spectra (DADS) are shown in Figure 2A–E and are overlaid in Figure 2F. The errors in the amplitudes of these spectra were small, and are indicated by the vertical lines in Figure 2A–E.

The 0.18 ps component (dotted in Figure 1, DADS in Figure 2A) exhibited an intense bleach around 810 nm and a broad absorbance increase around 870 nm. This component can (at least for a large part, see below) be assigned to the energy transfer process B*→P*, which occurs following excitation of the system in the B Q_y band at 800 nm (47, 48). The 1.9 ps component (dot-dashed in Figure 1, DADS in Figure 2B) showed a rather broad absorption increase around 800 nm, and a bleach centered at approximately 1020

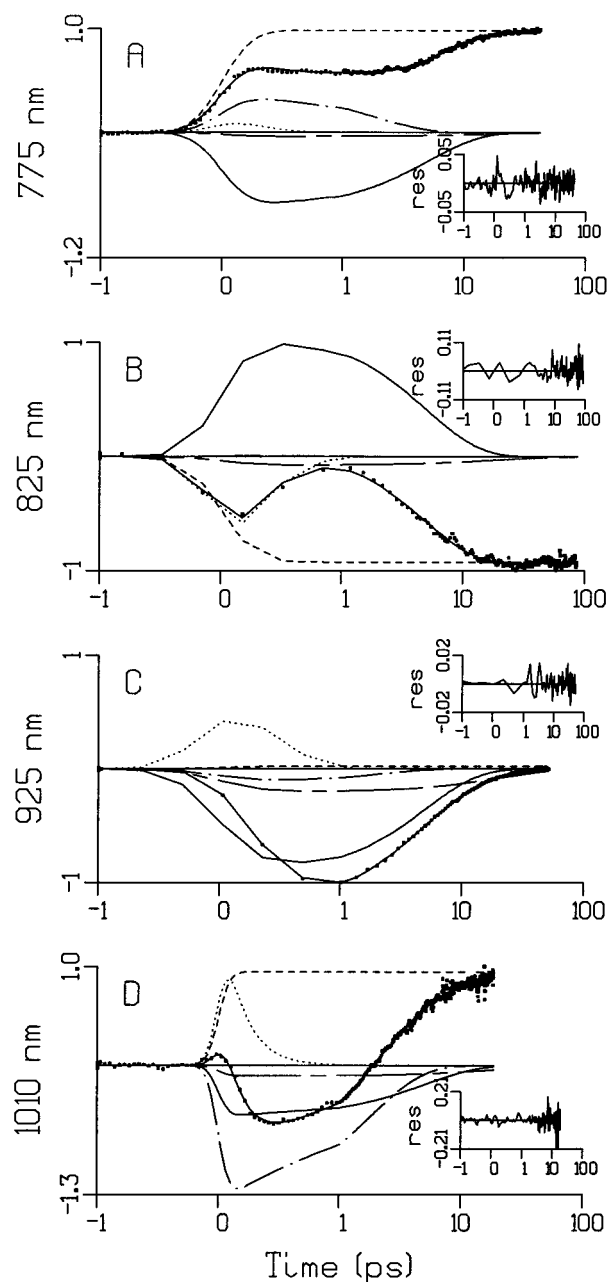


FIGURE 1: Global analysis of (normalized) kinetics in membrane bound wild type *Rb. sphaeroides* RCs measured at 775, 825, 925, and 1010 nm. Insets show residuals of a fit with five mono-exponential decays. The contributions of these decays to the fit are depicted by different line types. Key: 0.18 ps (dotted), 1.9 ps (dot-dashed), 5.1 ps (solid), 22 ps (chain dash), and long-lived (dashed). The sum of these contributions is also represented by a solid line through the measuring points. Note that the range and density of these points differ between the traces. The time base from -1 to +1 ps (relative to the maximum of the instrument response) is linear, and from 1 to 100 ps is logarithmic.

nm. This component gave a large contribution to the kinetic traces at 775 and 1010 nm (dot-dashed traces in Figure 1A,D). The 5.1 ps component (solid in Figure 1, DADS in Figure 2C) had a spectrum around 800 nm which had the opposite sign to that of the bandshift in the end spectrum (Figure 2E) and showed a broad bleach to the red of 860 nm which we assign to the stimulated emission from P*. The 22 ps component DADS (Figure 2D) showed an overall resemblance to the 5.1 ps DADS (Figure 2C) but had an amplitude that was a factor of 6 smaller. The contribution

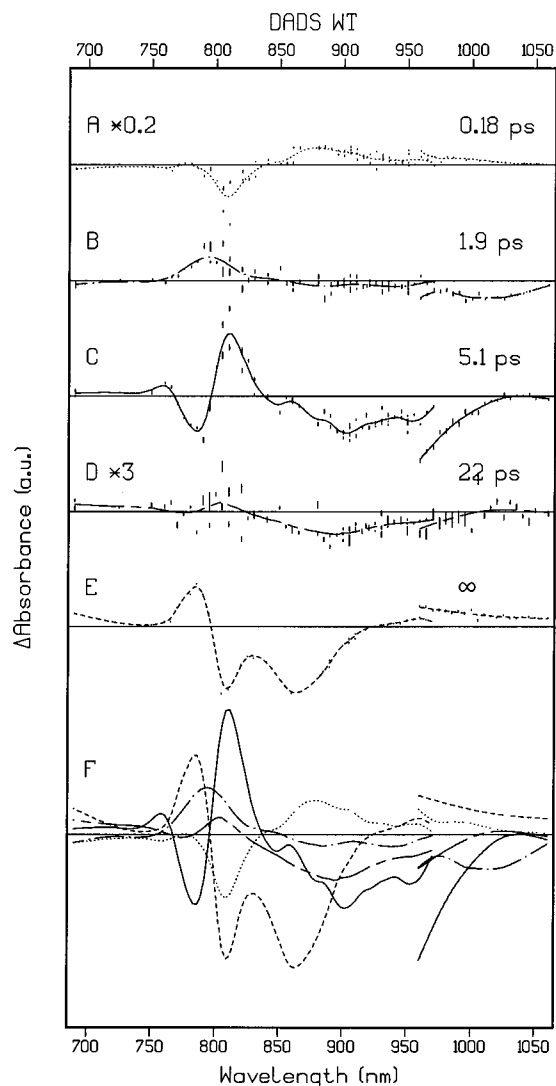


FIGURE 2: Decay-associated difference spectra (DADS) from global analysis with lifetimes of 0.18 ps (DADS divided by 5), 1.9 ps, 5.1 ps, 22 ps (DADS multiplied by 3), and long-lived. Vertical lines indicate plus or minus standard error in amplitude. Note that for clarity the amplitudes of the 960–1060 nm data set have been multiplied by 5. Key: 0.18 ps (A, dotted), 1.9 ps (B, dot-dashed), 5.1 ps (C, solid), 22 ps (D, chain dash), and long-lived (E, dashed). An overlay of the spectra is shown in (F); relative scaling is as for A–E.

of the 22 ps component to the kinetics in the P^* stimulated emission region is shown by the chain-dashed traces in Figure 1C,D. Below 810 nm the DADS of the 22 ps component differed somewhat from the DADS of the 5.1 ps component (Figure 2D, cf. Figure 2C).

Global Analysis of Light-Induced Absorption Changes in Membrane-Bound YM210H Mutant RCs

The optimum fit to the YM210H data yielded four lifetimes of 0.2, 3.1, and 12 ps and a long-lived component (Figure 3), and the corresponding DADS are shown in Figure 4. The 0.2 ps component can be ascribed to energy transfer from B^* to P^* , in line with the 0.18 ps component seen in the analysis of the wild type RC. The 3.1 ps and 12 ps components had similar DADS to the 5.1 and 22 ps components seen in the WT data (Figure 4B,C compared with Figure 2C,D). We therefore ascribe the 3.1 and 12 ps lifetimes to multi-exponential decay of the P^* state. How-

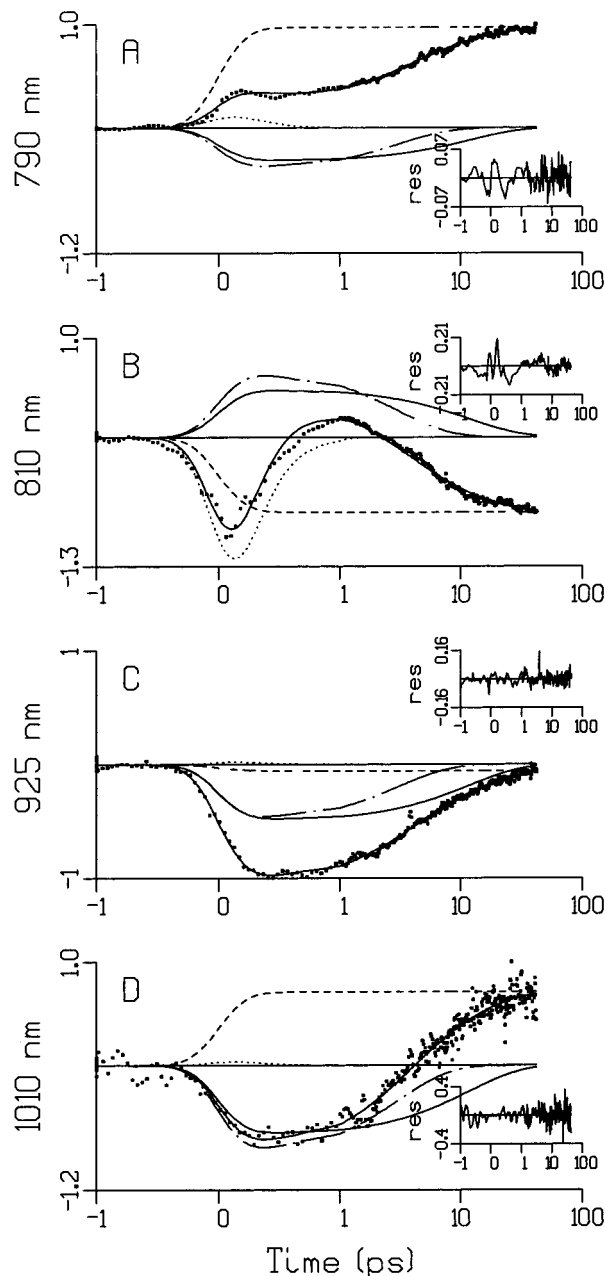


FIGURE 3: Global analysis of (normalized) kinetics in membrane-bound YM210H *Rb. sphaeroides* RCs measured at 790, 810, 925, and 1010 nm. Insets show residuals of a fit with four mono-exponential decays. The contributions of these decays to the fit are depicted by different line types. Key: 0.2 ps (dotted), 3.1 ps (dot-dashed), 12.0 ps (solid), and long-lived (dashed). The sum of these contributions is also represented by a solid line through the measuring points. The time base from -1 to +1 ps (relative to the maximum of the instrument response) is linear, and from 1 to 100 ps is logarithmic.

ever, in the 1000–1050 nm region the 3.1 ps component shows a larger bleach than the 12 ps component (compare dot-dashed and solid lines in Figure 4E).

DISCUSSION

Target Analysis of the WT RC Data with a Reaction Scheme Involving Radical Pair Relaxation

The global analysis of the wild type membrane bound RC data yielded five lifetimes and corresponding DADS. The 0.18 ps component was already attributed to the energy

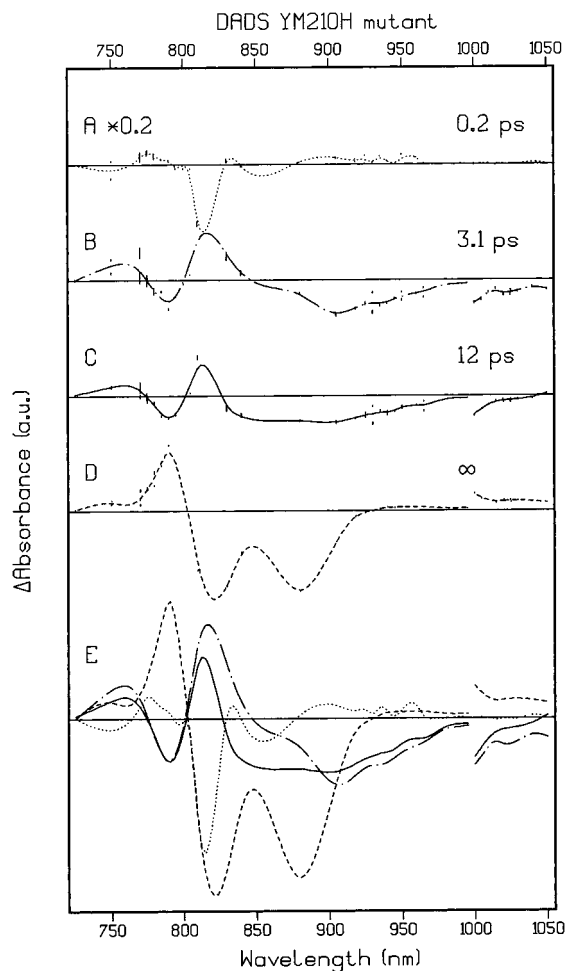


FIGURE 4: Decay-associated difference spectra (DADS) of membrane-bound YM210H reaction centers from global analysis with lifetimes of 0.2 ps (DADS divided by 5), 3.1 ps, 12.0 ps, and long-lived. Vertical lines indicate plus or minus standard error in amplitude. Note that for clarity the amplitudes of the 1000–1050 nm data have been multiplied by 5. Key: 0.2 ps (A, dotted), 3.1 ps (B, dot-dashed), 12.0 ps (C, solid), and long-lived (D, dashed). An overlay of the spectra is shown in (E); relative scaling is as for A–D.

transfer process $B^* \rightarrow P^*$, which occurs after excitation at 800 nm. The 1.9 ps DADS (Figure 2B) showed a negative contribution centered at 1020 nm. This is similar to the data presented by Zinth and co-workers (6, 12) who described a 0.9 ps component with a negative amplitude around 1020 nm in detergent-solubilized, wild type *Rb. sphaeroides* RCs. In accord with the conclusions in (6, 12), the 1020 nm bleach and the 1.9 ps component in the present study are ascribed to B_L^- as part of a $P^+B_L^-$ radical pair state. We also note the 1.5 ps lifetime reported in a study of the 500–940 nm spectral region by Holzwarth and Müller (18), which was also ascribed to the $P^+B_L^-$ state. The discrepancy in lifetimes (0.9 and 1.5 ps, cf. 1.9 ps in the present study) is possibly attributable to the reduction of Q_A in our studies, but not in the experiments described in (6, 12, 18). The overall decay of P^* was also found to slow down upon quinone reduction (7, 19). We ascribe the 5.1 ps lifetime to primary charge separation and thus arrive at the partial kinetic scheme $B^* \rightarrow P^* \rightarrow P^+B_L^- \rightarrow P^+H_L^-$. To accommodate the 22 ps lifetime we assume a relaxation of the second charge-separated state $P^+H_L^-$. To account for the multi-exponential nature of the decay of the P^* (stimulated) emission we

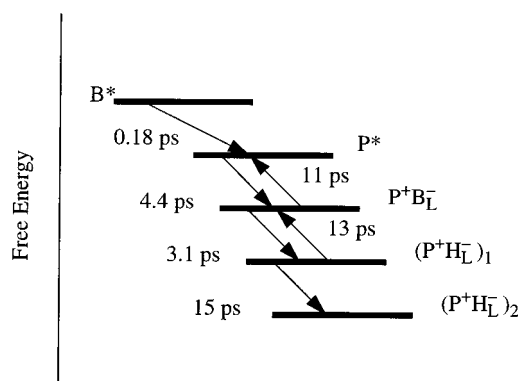


FIGURE 5: Compartmental scheme for energy transfer and charge transfer in the bacterial reaction center. Reciprocals of the inter-compartmental rates are written next to corresponding arrows. The lifetimes of this model, with the given time constants, are the same as those obtained from the five-component global analysis fit.

introduce back-reactions (18, 39, 40). Thus we arrive at the full kinetic scheme $B^* \rightarrow P^* \rightleftharpoons P^+B_L^- \rightleftharpoons (P^+H_L^-)_1 \rightarrow (P^+H_L^-)_2$.

To estimate the rate constants for the backward reactions we follow the same procedure as in ref 18. The decay part of the 925 nm kinetics (Figure 1C) is assumed to represent P^* decay, which according to the above kinetic scheme is triexponential. The amplitudes of the P^* decay in seventeen traces measured between 920 and 940 nm were estimated to be 1.9 ps (15%), 5.1 ps (70%), and 22 ps (15%). From these three lifetimes and relative amplitudes the reciprocals of the inter-compartmental rates shown in Figure 5 were calculated (49). Target analysis with the five-component kinetic scheme described above resulted in the same lifetimes and residuals as calculated in the global analysis. The species-associated difference spectra (SADS) (Figure 6) were consistent with the expected spectral properties of the intermediate states specified in the scheme. In particular, Figure 6C shows the 810 and 860 nm bleach, together with the positive band at 1020 nm, that would be expected for the radical pair state $P^+B_L^-$ (5, 8, 9, 12, 18). Note the difference of the 1020 nm band with the SADS of Figure 6D,E in the overlay Figure 6F. The SADS of the second state, supposedly P^* , showed stimulated emission in the 900 nm region superimposed on the bleach of the P_{Q_y} absorption band at 870 nm, and excited state absorption below 830 nm (Figure 6B). The amount of bleach of the P-band is the same for the three charge separated states (Figure 6C,D,E overlaid in Figure 6F). This is in contrast to the analysis of Holzwarth and Müller (18), where a similar model yielded a decrease of the P_{Q_y} bleach on going from the $P^+B_L^-$ state to the $P^+H_L^-$ state, which is inconsistent with the observed high quantum yield of charge separation.

The free energy differences estimated from this model are 24 meV between P^* and $P^+B_L^-$ and 37 meV between $P^+B_L^-$ and $(P^+H_L^-)_1$. These free energy differences were somewhat smaller than, respectively, 41 and 50 meV estimated in ref 18 from a similar analysis. These differences arise mainly from the faster forward reaction rates obtained in that study, resulting in lifetimes of 1.5 and 3.1 ps in ref 18 compared with 1.9 and 5.1 ps in the present study. The smaller free energy differences may be attributable to the use of Q_A -reduced RCs in the present work. Reduction of Q_A would be expected to raise the free energy of radical

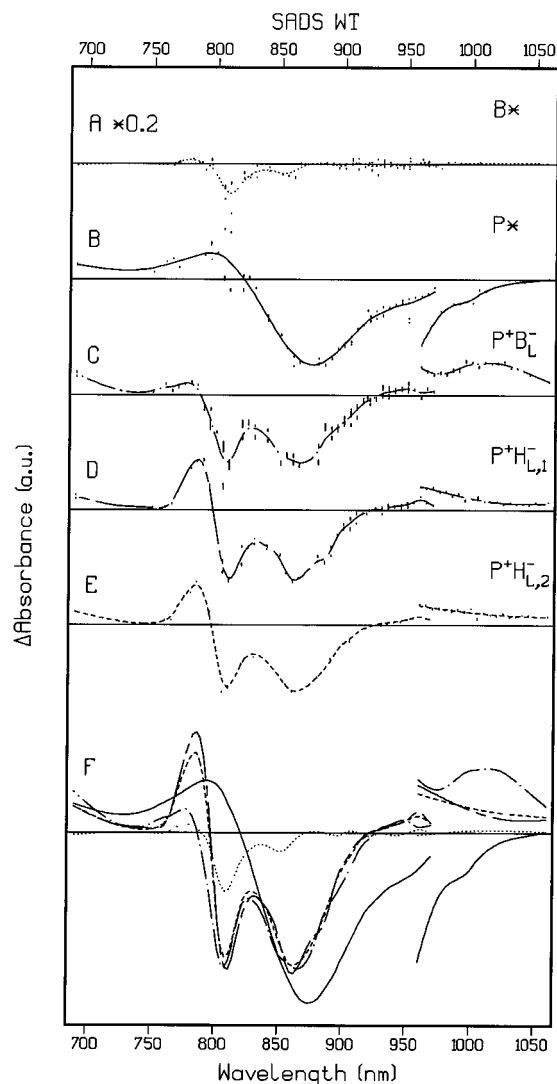


FIGURE 6: Species-associated difference spectra (SADS) from target analysis with lifetimes of 0.18, 1.9, 5.1, and 22 ps and long-lived. The compartmental scheme used in the target analysis is shown in Figure 5. Vertical lines indicate plus or minus standard error in amplitude. Note that for clarity the amplitudes of the 960–1060 nm data set have been multiplied by 5. Key: B^* (A, dotted, SADS divided by 5), P^* (B, solid), $P^+B_L^-$ (C, dot-dashed), $(P^+H_L^-)_1$ (D, chain-dash), and $(P^+H_L^-)_2$ (E, dashed). An overlay of the spectra is shown in F. Scaling is as in Figure 2.

pair states such as $P^+B_L^-$ and $P^+H_L^-$, decreasing the energy gap with P^* .

Target Analysis of the WT RC Data with a Branched Reaction Scheme Involving Charge Separation via B^*

Motivated by our observation of an efficient alternative pathway of charge separation via B^* at 77 K in *Rb. sphaeroides* RCs of the YM210W mutant (23, 24), of the heterodimer and of the wild type (Van Brederode et al., unpublished observations), we added a parallel $B^* \rightarrow P^+B_L^-$ path with a rate of 1/ps. Such a process would then also be consistent with the observed 15% decrease of P^* emission upon 800 nm excitation (relative to 860 nm excitation) measured at room temperature (20). The SADS of this target analysis (Figure 7) were similar to those from Figure 6, except for an increase of the P^* -stimulated emission and changes of the presumed P^* and $P^+B_L^-$ bands in the 800 nm region. In particular the B_L^- bleaching was more

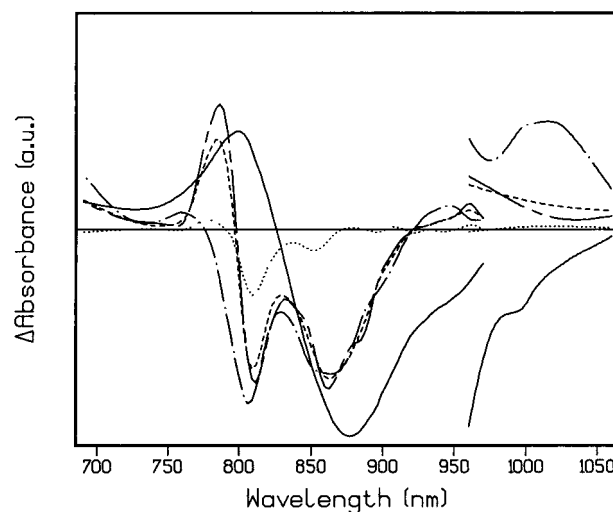


FIGURE 7: Species-associated difference spectra (SADS) from target analysis with compartmental scheme shown in Figure 5, except for a parallel $B^* \rightarrow P^+B_L^-$ path with a rate of 1/ps in addition to the $B^* \rightarrow P^*$ path with a rate of 4.65/ps. Note that for clarity the amplitudes of the 960–1060 nm data set have been multiplied by 5. Key: B^* (dotted, SADS divided by 5), P^* (solid), $P^+B_L^-$ (dot-dashed), $(P^+H_L^-)_1$ (chain-dash), and $(P^+H_L^-)_2$ (dashed). Scaling is as in Figure 2.

consistent with the expected spectral properties (dot-dashed in Figure 7). As a consequence, we believe that such a reaction scheme is very possible, also at room temperature.

Target Analysis of the WT RC Data with Three Mono-Exponential Decays and One Multi-Exponential Decay

The differences between the two putative $P^+H_L^-$ SADS (Figure 6D,E) were not very great. More data on different time scales, preferably with direct excitation of P and both with and without pre-reduction of Q_A , will be needed to test whether such a relaxation process is strictly required to provide an accurate description of the multi-exponential nature of the P^* stimulated emission decay. Several research groups have observed that the decay of stimulated and spontaneous emission from P^* is best described by a bi-exponential decay, or by a distribution of rate constants, and a variety of models have been presented to account for this that do not invoke radical pair relaxation (11, 19, 32–37). Given this, we examined whether a four component model could also provide an adequate description of the data. For one component a distribution of lifetimes is mimicked by a sum of four exponentials with fixed lifetimes of 2.5, 5, 10, and 20 ps. The three relative amplitude parameters of this sum have to be estimated. Note that we use here the term target analysis to express that our target is the multiexponential decay of one of the components. However, since all components decay independently we still speak of DADS. Moving from a model with five mono-exponential decays and corresponding DADS to a model with three mono-exponential decays, one four-exponential decay and corresponding DADS reduced the number of free parameters significantly, replacing one DADS of 97 parameters by three amplitude parameters for the four-exponential. The fit of the target analysis to the kinetic data at the four sample wavelengths is shown in Figure 8 and should be compared with the fit to the same data shown in Figure 1. Although

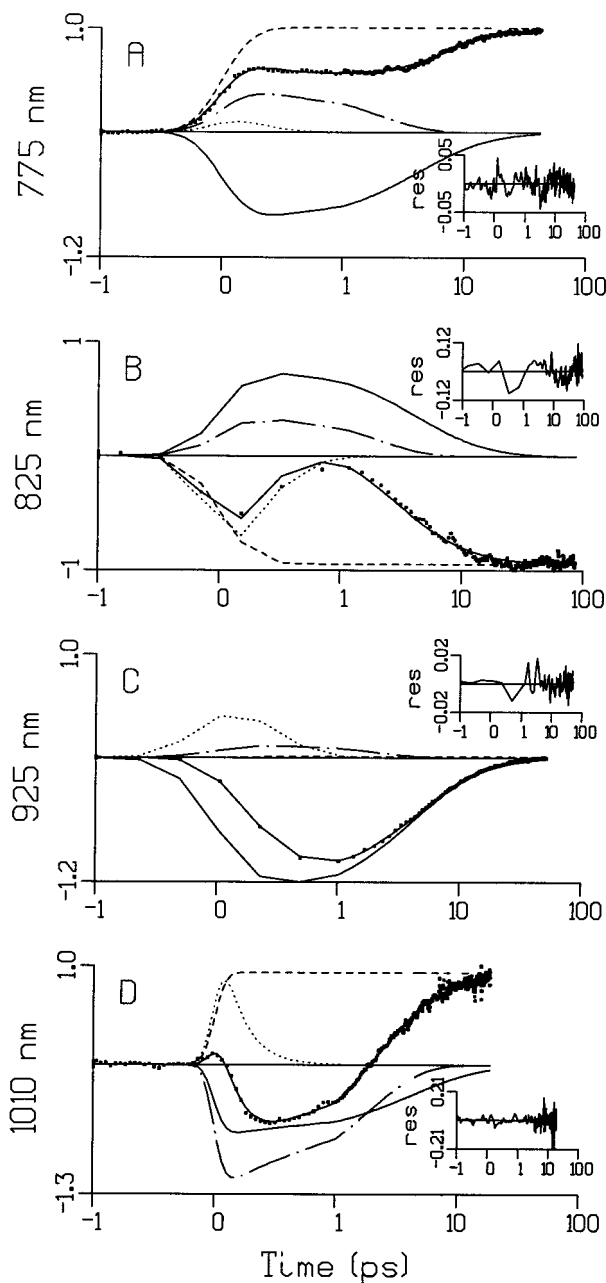


FIGURE 8: Target analysis of (normalized) kinetics in membrane bound WT RCs measured at 775, 825, 925, and 1010 nm. Insets show residuals of a fit with one four-exponential decay plus three mono-exponential decays. The contributions of these decays to the fit are depicted with different line types. Key: 0.18 ps (dotted), 1.9 ps (dot-dashed), four exponential consisting of 2.5 ps (amplitude 26%), 5 ps (54%), 10 ps (10%), and 20 ps (10%) (solid) and long-lived (dashed). The sum of these contributions is also represented by a solid line through the measuring points. Note that the range and density of these points differ between the traces. The time base from -1 to $+1$ ps (relative to the maximum of the instrument response) is linear, and from 1 to 100 ps is logarithmic.

the fit illustrated in Figure 8 was still quite good, small trends in the residuals were visible; compare the insets in Figure 1 to those in Figure 8. The weighted root mean square (rms) error increased by 7% relative to the five-component fit. For comparison, a global analysis (results not shown) in which the four-exponential decay was replaced by a single mono-exponential decay resulted in an increase of the weighted rms error by 16% relative to the five-component fit. Compared to the fit with five components, the short lifetimes do not change, and the four-exponential decay component

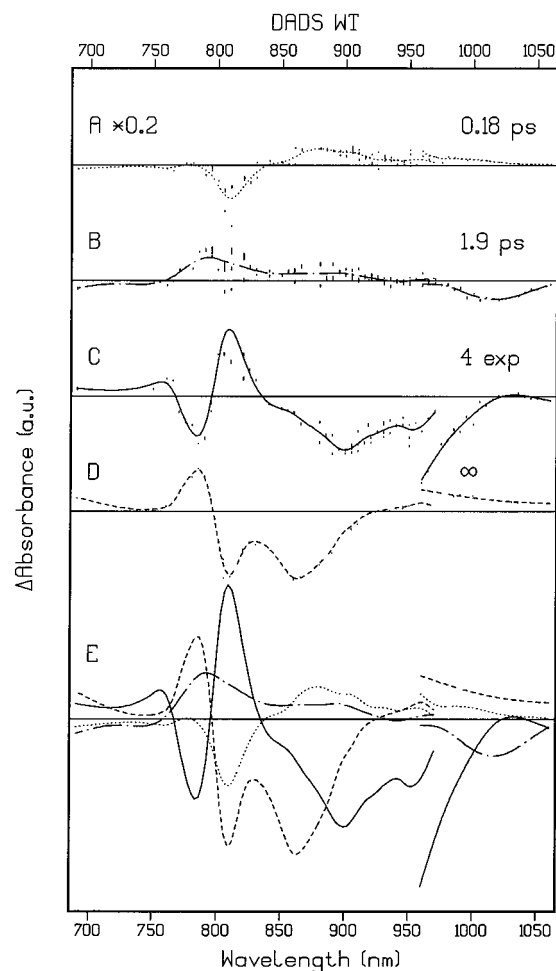


FIGURE 9: Decay-associated difference spectra (DADS) from target analysis with one four-exponential decay plus three mono-exponential decays. Key: 0.18 ps (A, dotted, DADS divided by 5), 1.9 ps (B, dot-dashed), four-exponential consisting of 2.5 ps (amplitude 26%), 5 ps (54%), 10 ps (10%), and 20 ps (10%) (C, solid) and long-lived (D, dashed). Vertical lines indicate plus or minus standard error in amplitude. Note that for clarity the amplitudes of the 960–1060 nm data set have been multiplied by 5. An overlay of the spectra is shown in E. Scaling is as in Figure 2.

is estimated to consist of 2.5 ps (amplitude 26%), 5 ps (54%), 10 ps (10%), and 20 ps (10%) which is skewed toward the longer lifetimes. Clear changes have now become visible in the DADS of the 1.9 ps component, compare Figure 9B with Figure 2B. In the near-infrared a nicely shaped band has appeared because the stimulated emission amplitude that was present in the DADS of Figure 2B has disappeared. It can be shown analytically (see Supporting Information) that, assuming a heterogeneous sequential model without back reactions, the DADS of the 1.9 ps component is proportional to the difference between the SADS of $P^+H_L^-$ and $P^+B_L^-$. Assuming that H_L^- does not absorb around 1020 nm, the band centered at this wavelength in Figure 9B represents the shape of the B_L^- absorption band. The amplitude in the 900–950 nm region is almost zero. This analysis strongly suggests that the $P^+B_L^-$ population decays with 1.9 ps, and that if this state is involved in equilibria, then its population becomes so small that it is no longer detectable with the present signal to noise ratio. Furthermore, the 26% amplitude of the 2.5 ps part of the four-exponential decay clearly indicates that short lifetime components are present in the

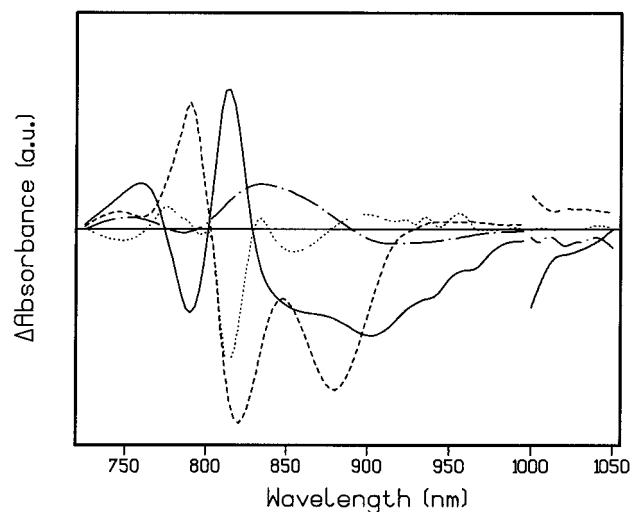


FIGURE 10: Decay-associated difference spectra (DADS) of membrane-bound YM210H reaction centers from target analysis with one four-exponential decay plus three mono-exponential decays. Key: 0.2 ps (dotted, DADS divided by 5), 2.2 ps (dot-dashed), four exponential consisting of 3 ps (amplitude 29%), 6 ps (38%), 12 ps (18%), and 24 ps (15%) (solid) and long-lived (dashed). Note that for clarity the amplitudes of the 1000–1050 nm data have been multiplied by 5. Scaling is as in Figure 4.

P^* decay, which is corroborated by the 15% amplitude of the 1.9 ps P^* decay found with the scheme from Figure 5, and which is in accordance with the 30% amplitude of the 1.5 ps P^* decay reported in ref 18.

Comparison of Global Analysis Results from Membrane-Bound WT and YM210H Mutant RCs

It was noticeable in the YM210H data that the relative amplitude of the 12 ps component of the P^* decay was significantly larger than that of the 22 ps component in the corresponding data for the WT complex. This can be seen by comparing Figure 4C with Figure 2D, remembering that in the latter the DADS was multiplied by 3 for the purpose of comparison. This pattern of shorter lifetimes but a greater relative amplitude for the slowest component of P^* decay in the YM210H membranes is consistent with our findings in a previous report, where a multi-exponential fit was made to kinetic data recorded at 920 nm in wild type and YM210H membrane-bound RCs (without pre-reduction of Q_A) (19). Analysis of these single wavelength data yielded lifetimes (and percentage amplitudes) of 2.1 ps (40%) and 8.2 ps (60%) for the YM210H membranes as compared with 3.9 ps (90%) and 16.1 ps (10%) for wild type membranes.

The global analysis of the YM210H data did not yield a lifetime equivalent to the 1.9 ps lifetime seen in the wild type data, which we attribute to a $P^+B_L^-$ radical pair state (vide supra). We tried to resolve another fast lifetime using a model with three mono-exponential decays and one four-exponential decay (with fixed lifetimes), analogous to the previous section. The four-exponential decay component is estimated to consist of 3 ps (amplitude 29%), 6 ps (38%), 12 ps (18%), and 24 ps (15%) which is again skewed toward the longer lifetimes. We now find an additional component with a lifetime of 2.2 ps. Its DADS (dot-dashed in Figure 10) contains a bleach around 1020 nm. Note that this DADS resembles the difference of the 3.1 ps and 12 ps DADS of Figure 4B,C. Analogous to the band centered at 1020 nm in Figure 9B (vide supra), this probably is evidence for a

$P^+B_L^-$ intermediate, with a lifetime close to the shortest lifetime of P^* decay. Measurements with a higher signal to noise ratio are necessary to further support this.

Implications of Our Findings for the Mechanism of Primary Charge Separation from P^* in WT RCs

The data and analysis presented in this report are aimed at addressing two key questions concerning the mechanism of the first step of light-driven electron transfer in RCs. The first concerns the much debated role of the accessory BChl B_L , and specifically the proposal that the $P^+B_L^-$ radical pair state is formed as a true intermediate during electron transfer from P^* to $P^+H_L^-$ (5, 6, 8, 9, 12, 18). The analysis presented in this paper is entirely consistent with the view that the $P^+B_L^-$ state is formed as a detectable intermediate, with in our case a lifetime of 1.9 ps in Q_A -reduced, membrane-bound wild type *Rb. sphaeroides* RCs. The SADS of the $P^+B_L^-$ intermediate state had the expected features, with a bleach of the B and PQ_y absorption bands at 810 and 860 nm, respectively, and formation of an anion absorption band at 1020 nm (Figure 6C,F). Note also the nicely shaped band around 1020 nm in Figure 9B.

The second question we have sought to address concerns the origin of the complex decay of the P^* state. The most favourable fit to the full set of experimental data from 690–1060 nm required five lifetimes. A combination of the model for RC kinetics from (5, 6, 8, 9, 12, 18) and the idea of radical pair relaxation (5, 18, 38–40) gave a five-component kinetic scheme (Figure 5) that offered a satisfactory description of the data. The SADS of the two excited states and three radical pair states involved in this scheme were consistent with what is known about the spectra of these states. However, whether or not five components with different spectra were absolutely needed for an adequate description of the data could not be decided, because the differences in the SADS for radical pair states $(P^+H_L^-)_1$ and $(P^+H_L^-)_2$ were not large enough to identify these as discrete components with sufficient certainty. Decreasing the number of components used in the global analysis from five to four (one of these being a multi-exponential decay) reduced the quality of the fit to the experimental data, causing a 7% increase in the weighted rms error. However, this simplified fit was still quite good (see Figure 8) and so may be acceptable. Several compartmental schemes are possible for this four component model, involving heterogeneous kinetics. However, more accurate measurements of the RC dynamics (in particular the P^* emission) at different temperatures, excitation wavelengths, and over several time scales are needed to decide how to include the aspects of relaxation and distributed kinetics or heterogeneity. Finally, we have shown that a target analysis including the direct process $B^* \rightarrow P^+B_L^-$ bypassing P^* is a viable possibility (Figure 7). In the near future we will further substantiate the decay processes following excitation of B^* at room temperature.

SUPPORTING INFORMATION AVAILABLE

Analytical derivation that, assuming a heterogeneous sequential model without back reactions, the DADS of the 1.9 ps component in Figure 9B is proportional to the difference between the SADS of $P^+H_L^-$ and $P^+B_L^-$ (2 pages). Ordering information is given on any current masthead page.

REFERENCES

1. Deisenhofer, J., Epp, O., Miki, K., Huber, R., and Michel, H. (1985) *Nature* 318, 618–624.
2. Feher, G., Allen, J. P., Okamura, M. Y., and Rees, D. C. (1989) *Nature* 339, 111–116.
3. Kirmaier, C., Holten, D., and Parson, W. W. (1985) *Biochim. Biophys. Acta* 810, 49–61.
4. Kirmaier, C., and Holten, D. (1987) *Photosynth. Res.* 13, 225–260.
5. Woodbury, N. W., and Allen, J. P. (1995) in *Anoxygenic Photosynthetic Bacteria* (Blankenship, R. E., Madigan, M. T., and Bauer, C. E., Eds.) pp 527–557, Kluwer Academic Publishers, Dordrecht, The Netherlands.
6. Schmidt, S., Arlt, T., Hamm, P., Lauterwasser, C., Finkle, U., Drews, G., and Zinth, W. (1993) *Biochim. Biophys. Acta* 1144, 385–390.
7. Beekman, L. M. P., Visschers, R. W., Monshouwer, R., Heer-Dawson, M., Mattioli, T. A., McGlynn, P., Hunter, C. N., Robert, B., Van Stokkum, I. H. M., Van Grondelle, R., and Jones, M. R. (1995) *Biochemistry* 34, 14712–14721.
8. Holzapfel, W., Finkle, U., Kaiser, W., Oesterheld, D., Scheer, H., Stülz, H. U., and Zinth, W. (1989) *Chem. Phys. Lett.* 160, 1–7.
9. Holzapfel, W., Finkle, U., Kaiser, W., Oesterheld, D., Scheer, H., Stülz, H. U., and Zinth, W. (1990) *Proc. Natl. Acad. Sci. U.S.A.* 87, 5168–5172.
10. Kirmaier, C., and Holten, D. (1991) *Biochemistry* 31, 609–613.
11. Kirmaier, C., and Holten, D. (1990) *Proc. Natl. Acad. Sci. U.S.A.* 87, 3552–3556.
12. Arlt, T., Schmidt, S., Kaiser, W., Lauterwasser, C., Meyer, M., Scheer, H., and Zinth, W. (1993) *Proc. Natl. Acad. Sci. U.S.A.* 90, 11757–11761.
13. Du, M., Rosenthal, S. J., Xie, X., DiMagno, T. J., Schmidt, M., Hanson, D. K., Schiffer, M., Norris, J. R., and Fleming, G. R. (1992) *Proc. Natl. Acad. Sci. U.S.A.* 89, 8517–8521.
14. Hamm, P., Gray, K. A., Oesterheld, D., Feick, R., Scheer, H., and Zinth, W. (1993) *Biochim. Biophys. Acta* 1142, 99–105.
15. Jia, Y., DiMagno, T. J., Chan, C.-K., Wang, Z., Du, M., Hanson, D. K., Schiffer, M., Norris, J. R., Fleming, G. R., and Popov, M. S. (1993) *J. Phys. Chem.* 97, 13180–13191.
16. Vos, M. H., Lambry, J.-C., Robles, S. J., Youvan, D. C., Breton, J., and Martin, J.-L. (1991) *Proc. Natl. Acad. Sci. U.S.A.* 88, 8885–8889.
17. Vos, M. H., Jones, M. R., Breton, J., Lambry, J.-C., and Martin, J.-L. (1996) *Biochemistry* 35, 2687–2692.
18. Holzwarth, A. R., and Müller, M. G. (1996) *Biochemistry* 35, 11820–11831.
19. Beekman, L. M. P., Van Stokkum, I. H. M., Monshouwer, R., Rijnders, A. J., McGlynn, P., Visschers, R. W., Jones, M. R., and Van Grondelle, R. (1996) *J. Phys. Chem.* 100, 7256–7268.
20. Lin, S., Taguchi, A. K. W., and Woodbury, N. W. (1996) *J. Phys. Chem.* 100, 17067–17078.
21. Schmidt, S., Arlt, T., Hamm, P., Huber, H., Nägele, T., Wachtveitl, J., Meyer, M., Scheer, H., and Zinth, W. (1994) *Chem. Phys. Lett.* 223, 116–120.
22. Arlt, T., Bibikova, M., Penzkofer, H., Oesterheld, D., and Zinth, W. (1996) *J. Phys. Chem.* 100, 12060–12065.
23. Van Brederode, M. E., Jones, M. R., and Van Grondelle, R. (1997) *Chem. Phys. Lett.* 268, 143–149.
24. Van Brederode, M. E., Jones, M. R., Van Mourik, F., Van Stokkum, I. H. M., and Van Grondelle, R. (1997) *Biochemistry* 36, 6855–6861.
25. Parson, W. W., Chu, Z.-T., and Warshel, A. (1990) *Biochim. Biophys. Acta* 1017, 251–272.
26. Heller, B. A., Holten, D., and Kirmaier, C. (1995) *Science* 269, 940–945.
27. Gunner, M. R., Nicholls, A., and Honig, B. (1996) *J. Phys. Chem.* 100, 4277–4291.
28. Alden, R. G., Parson, W. W., Chu, Z. T., and Warshel, A. (1996) *J. Phys. Chem.* 100, 16761–16770.
29. Stocker, J. W., Taguchi, A. K. W., Muchison, H. A., Woodbury, N. W., and Boxer, S. G. (1992) *Biochemistry* 31, 10356–10362.
30. Williams, J. C., Alden, R. G., Murchison, H. A., Peloquin, J. M., Woodbury, N. W., and Allen, J. P. (1992) *Biochemistry* 31, 11029–11037.
31. Murchison, H. A., Alden, R. G., Allen, J. P., Peloquin, J. M., Taguchi, A. K. W., Woodbury, N. W., and Williams, J. C. (1993) *Biochemistry* 32, 3498–3505.
32. Jia, Y., DiMagno, T. J., Chan, C.-K., Wang, Z., Du, M., Hanson, D. K., Schiffer, M., Norris, J. R., Fleming, G. R., and Popov, M. S. (1993) *J. Phys. Chem.* 97, 13180–13191.
33. Ogrodnik, A., Keupp, W., Volk, M., Aumeier, G., and Michel-Beyerle, M. E. (1994) *J. Phys. Chem.* 98, 3432–3439.
34. Small, G. J., Hayes, J. M., and Silbey, R. J. (1992) *J. Phys. Chem.* 96, 7499–7501.
35. Gudowska-Nowak, E. (1994) *J. Phys. Chem.* 98, 5257–5264.
36. Wang, Z., Pearlstein, R. M., Jia, Y., Fleming, G. R., and Norris, J. R. (1993) *Chem. Phys.* 176, 421–425.
37. Bixon, M., Jortner, J., and Michel-Beyerle, M. E. (1995) *Chem. Phys.* 197, 389–404.
38. Peloquin, J. M., Williams, A. C., Lin, X., Alden, R. G., Taguchi, A. K. W., Allen, J. P., and Woodbury, N. W. (1994) *Biochemistry* 33, 8089–8100.
39. Woodbury, N. W., and Parson, W. W. (1984) *Biochim. Biophys. Acta* 767, 345–361.
40. Woodbury, N. W., and Parson, W. W. (1986) *Biochim. Biophys. Acta* 850, 197–210.
41. Beekman, L. M. P., Jones, M. R., Van Stokkum, I. H. M., and Van Grondelle, R. (1995) in *Photosynthesis: From Light to Biosphere* (Mathis, P., Ed.) Vol. 1, pp 495–498, Kluwer Academic Publishers, Dordrecht, The Netherlands.
42. Jones, M. R., Heer-Dawson, M., Mattioli, T. A., Hunter, C. N., and Robert, B. (1994) *FEBS Lett.* 339, 18–24.
43. Van Stokkum, I. H. M., Brouwer, A. M., Van Ramesdonk, H. J., and Scherer, T. (1993) *Proc. K. Ned. Acad. Wet.* 96, 43–68.
44. Breton, J., Nabedryk, E., and Parson, W. W. (1992) *Biochemistry* 31, 7503.
45. Breton, J. (1985) *Biochim. Biophys. Acta* 810, 235–245.
46. *International Mathematical and Statistical Libraries*, Visual Numerics, Inc., Houston, TX.
47. Jia, Y., Jonas, D. M., Joo, T., Nagasawa, Y., Lang, M. J., and Fleming, G. R. (1995) *J. Phys. Chem.* 99, 6263–6266.
48. Stanley, R. J., King, B., and Boxer, S. G. (1996) *J. Phys. Chem.* 100, 12052–12059.
49. Godfrey, K. (1983) *Compartmental Models and Their Application*, pp 58–65, Academic Press, London.
50. Nagle, J. F., Parodi, L. A., and Lozier, R. H. (1982) *Biophys. J.* 38, 161–174.

BI9707943